JNeurosci
THE JOURNAL OF NEUROSCIENCE

Research Articles: Neurobiology of Disease

TNF-α differentially regulates synaptic plasticity in the hippocampus and spinal cord by microglia-dependent mechanisms after peripheral nerve injury

Yong Liu[1,2,3,†], Li-Jun Zhou[1,2,†], Jun Wang[1,†], Dai Li[1], Wen-Jie Ren[1], Jiyun Peng[2,6], Xiao Wei[1], Ting Xu[1], Wen-Jun Xin[1,7], Rui-Ping Pang[1], Yong-Yong Li[1], Zhi-Hai Qin[5], Madhuvika Murugan[2,6], Mark P. Mattson[3,4], Long-Jun Wu[2,6] and Xian-Guo Liu[1,7]

[1]*Pain Research Center and Department of Physiology, Zhongshan School of Medicine of Sun Yat-sen University, Guangzhou 510080, China.*

[2]*Department of Cell Biology and Neuroscience, Rutgers University, Piscataway, NJ 08854, USA.*

[3]*Laboratory of Neurosciences, National Institute on Aging Intramural Research Program, Baltimore, MD 21224, USA.*

[4]*Department of Neuroscience, Johns Hopkins University School of Medicine, Baltimore, MD 21205, USA.*

[5]*National Laboratory of Biomacromolecules, Chinese Academy of Sciences- University of Tokyo Joint Laboratory of Structural Virology and Immunology, China.*

[6]*Department of Neurology, Mayo Clinic, Rochester, MN 55905, USA*

[7]*Guangdong Provincial Key Laboratory of Brain Function and Disease, China.*

DOI: 10.1523/JNEUROSCI.2235-16.2016

Received: 13 July 2016

Revised: 18 November 2016

Accepted: 2 December 2016

Published: 20 December 2016

Author contributions: Y. Liu, Z.L.-J., J.W., M.P.M., L.-J.W., and X.-G.L. designed research; Y. Liu, Z.L.-J., J.W., D.L., W.R., J.P., X.W., T.X., W.X., R.P., Y. Li, and M.M. performed research; Y. Liu, Z.L.-J., J.W., and Z.-H.Q. contributed unpublished reagents/analytic tools; Y. Liu, Z.L.-J., J.W., D.L., and W.R. analyzed data; Y. Liu, Z.L.-J., J.W., M.P.M., L.-J.W., and X.-G.L. wrote the paper.

Conflict of Interest: The authors declare no conflict of interest.

[†]These authors contributed equally to this work.

We thank Dr. Wen-Biao Gan for providing *CX3CR1CreER/+* mice and Huai-Yu Gu for technical support. This work was supported by grants from the National Natural Science Foundation of China (U1201223, 81200856, 30970957, 81371198 and 31000489), National Institute of Health (R01NS088627 and R21DE025689) and the Intramural Research Program of the National Institute on Aging.

Correspondence should be addressed to To whom correspondence should be addressed: liuxg@mail.sysu.edu.cn (X.G.L,) and lwu@dls.rutgers.edu (L.J.W.).

Cite as: J. Neurosci 2016; 10.1523/JNEUROSCI.2235-16.2016

Title: TNF-α differentially regulates synaptic plasticity in the hippocampus and spinal cord by microglia-dependent mechanisms after peripheral nerve injury

Abbreviated title: TNF-α and neural reorganization in pain

Authors: Yong Liu†[1,2,3], Li-Jun. Zhou†[1,2], Jun Wang†[1], Dai Li[1], Wen-Jie Ren[1], Jiyun Peng[2,6], Xiao Wei[1], Ting Xu[1], Wen-Jun Xin[1,7], Rui-Ping Pang[1], Yong-Yong Li[1], Zhi-Hai Qin[5], Madhuvika Murugan[2,6], Mark P. Mattson[3,4], Long-Jun Wu*[2,6] and Xian-Guo Liu*[1,7]

Affiliations:

[1] Pain Research Center and Department of Physiology, Zhongshan School of Medicine of Sun Yat-sen University, Guangzhou 510080, China.

[2]Department of Cell Biology and Neuroscience, Rutgers University, Piscataway, NJ 08854, USA.

[3]Laboratory of Neurosciences, National Institute on Aging Intramural Research Program, Baltimore, MD 21224, USA.

[4]Department of Neuroscience, Johns Hopkins University School of Medicine, Baltimore, MD 21205, USA.

[5]National Laboratory of Biomacromolecules, Chinese Academy of Sciences- University of Tokyo Joint Laboratory of Structural Virology and Immunology, China.

[6]Department of Neurology, Mayo Clinic, Rochester, MN 55905, USA

[7]Guangdong Provincial Key Laboratory of Brain Function and Disease, China.

†These authors contributed equally to this work.

*To whom correspondence should be addressed: liuxg@mail.sysu.edu.cn (X.G.L,) and lwu@dls.rutgers.edu (L.J.W.).

Number of pages: 39

Number of figures: 7

Number of words for

Abstract: 249

Introduction: 437

Discussion: 1163

Conflict of Interest

The authors declare no conflict of interest.

Acknowledgments

We thank Dr. Wen-Biao Gan for providing *CX3CR1*$^{CreER/+}$ mice and Huai-Yu Gu for technical support. This work was supported by grants from the National Natural Science Foundation of China (U1201223, 81200856, 30970957, 81371198 and 31000489), National Institute of Health (R01NS088627 and R21DE025689) and the Intramural Research Program of the National Institute on Aging.

Abstract

Clinical studies show that chronic pain is accompanied by memory deficits and reduction in hippocampal volume. Experimental studies show that spared nerve injury (SNI) of sciatic nerve induces long-term potentiation (LTP) at C-fiber synapses in spinal dorsal horn but impairs LTP in hippocampus. The opposite changes may contribute to neuropathic pain and memory deficits, respectively. However, the cellular and molecular mechanisms underlying the functional synaptic changes are unclear. Here we show that the dendrite lengths and spine densities are significantly reduced in hippocampal CA1 pyramidal neurons but increased in spinal neurokinin-1-positive neurons in mice after SNI, indicating that the excitatory synaptic connectivity is reduced in hippocampus but enhanced in spinal dorsal horn in this neuropathic pain model. Mechanistically, tumor necrosis factor-α (TNF-α) is up-regulated in bilateral hippocampus and in ipsilateral spinal dorsal horn, while brain derived neurotrophic factor (BDNF) is decreased in the hippocampus but increased in the ipsilateral spinal dorsal horn following SNI. Importantly, the SNI-induced opposite changes in synaptic connectivity and BDNF expression are prevented by genetic deletion of TNF receptor 1 *in vivo* and are mimicked by TNF-α in cultured slices. Furthermore, SNI activated microglia in both spinal dorsal horn and hippocampus; pharmacological inhibition or genetic ablation of microglia prevented the region-dependent synaptic changes, neuropathic pain and memory deficits induced by SNI. The data suggest that neuropathic pain involves different structural synaptic alterations in

spinal and hippocampal neurons that are mediated by overproduction of TNF-α and microglial activation, and may underlie chronic pain and memory deficits.

Significance Statement

Chronic pain is often accompanied by memory deficits. Previous studies show that peripheral nerve injury, produces both neuropathic pain and memory deficits, induces LTP at C-fiber synapses in spinal dorsal horn (SDH) but inhibits LTP in hippocampus. The opposite changes in synaptic plasticity may contribute to chronic pain and memory deficits, respectively. However, the structural and molecular bases of these alterations of synaptic plasticity are unclear. Here, we show that the complexity of excitatory synaptic connectivity and BDNF expression are enhanced in SDH but reduced in the hippocampus in neuropathic pain and the opposite changes depend on TNF-α /TNFR1 signaling and microglial activation. The region-dependent synaptic alterations may underlie chronic neuropathic pain and memory deficits induced by peripheral nerve injury.

Introduction

Chronic pain affects ~20% of the population and nearly 70% of those patients suffer from working memory deficits (Hart et al., 2000; Dick and Rashiq, 2007). The mechanism underlying the comorbidity of chronic pain and memory deficits is poorly understood. It has been proposed that pain-related sensory inputs may affect memory by disrupting attention, which is important for working memory formation (Eccleston, 1995; Awh et al., 2006). However, recent clinical studies show that the hippocampal volume is reduced in chronic pain patients, including those with chronic back pain, complex regional pain syndrome (Mutso et al., 2012) and knee osteoarthritis (Mao et al., 2016), suggesting that neuronal dystrophy in the hippocampus may contribute to memory deficits in chronic pain disorders. Experimental studies show that peripheral nerve injury, which induces chronic neuropathic pain (Decosterd and Woolf, 2000) and memory deficits in rodents (Ren et al., 2011), induces LTP at C-fiber synapses in spinal dorsal horn (Zhang et al., 2004), but impairs LTP at CA3-CA1 synapses in hippocampus (Ren et al., 2011). The data suggest that the synaptic plasticity is reduced in hippocampus but enhanced in spinal dorsal horn in neuropathic pain condition. The region-dependent synaptic plastic changes may contribute the chronic pain and memory deficits, respectively. However, the cellular and molecular mechanisms underlying the changes are still unclear.

It has been well established that microglial activation and elevated tumor necrosis factor-α (TNF-α) critically involved in both hippocampus-dependent cognitive deficit (Griffin et al., 2006; Rowan et al., 2007) and neuropathic pain induced by nerve injury (Xu et al., 2006; Ji and Suter, 2007). Similar to peripheral nerve injury, microglial activation and TNF-α overproduction inhibits LTP in hippocampus (Pickering et al., 2005;

Griffin et al., 2006) but is essential for the induction of spinal LTP at C-fiber synapses (Zhong et al., 2010; Wu et al., 2014). However, how can microglial activation and overproduction of TNF-α oppositely regulate the synaptic plasticity in hippocampus and spinal dorsal horn remains elusive.

Furthermore, chronic pain and memory deficits in human patients and in animals are long-lasing, which cannot be explained by the functional change in synaptic transmission. In the present work, we tested the hypothesis that the functional changes in synaptic plasticity initiated by peripheral nerve injury may transfer to structural synaptic alterations in the two regions. Indeed, we found that the structural and functional synaptic connections were enhanced in spinal dorsal horn but reduced in hippocampus in 7-10d after SNI in mouse. These opposite structural changes were prevented by deletion of TNFR1 and by inhibtion or ablation of microglia. The region-dependent structural synaptic alterations may underlie the chronic neuropathic pain and associated cognitive disorders.

Materials and Methods

Animals

Adult male C57BL/6 mice, *CX3CR1*$^{CreER/+}$ mice were used as wild type controls. Adult male TNFR1-knockout (TNFR1 KO, RRID:IMSR_JAX:003242) C57BL/6 and CX3CR1-EGFP mice were purchased from the Jackson Laboratories. *CX3CR1*$^{CreER/+}$ mice were obtained from Dr. Wen-Biao Gan at New York University. The mice were crossed with *R26*$^{iDTR/+}$ (purchased from Jackson's laboratory) to obtain *CX3CR1*$^{CreER/+}$*:* *R26*$^{iDTR/+}$ mice. Sprague Dawley rats (8-10 day-old) were used for hippocampus or spinal slice culture. The animals were housed in separated cages with access to food and water ad libitum. The room was kept at 23 ± 1°C and 50–60% humidity, under a light cycle (6:00 to 18:00 hours). All experimental procedures were approved by the Local Animal Care Committee and conformed to Chinese guidelines and Rutgers University on the ethical use of animals and all efforts were made to minimize the number of animals used and their suffering.

Spared nerve injury (SNI) and behavioral tests

The SNI was carried out following the procedures described previously(Decosterd and Woolf, 2000). Briefly, under anesthesia with chloral hydrate (0.4 g/kg, i.p.) the common peroneal and the tibial nerves were explored and tightly ligated with 5-0 silk and transected distal to the ligation, removing a 2–4 mm length of each nerve. Great care was taken to avoid any contact with or stretching of the intact sural nerve. The wound was closed in two layers.

Mechanical allodynia was assessed using von Frey hairs with the up-down method.

Briefly, the animals were placed under separate transparent Plexiglas chambers positioned on a wire mesh floor. 10~15 minutes were allowed for habituation. Each stimulus consisted of a 6–8 s application of a von Frey hair to the lateral surface of the foot with 5 min interval between stimuli. Quick withdrawal or licking of the paw in response to the stimulus was considered as a positive response.

Short-term memory (STM) was accessed by novel object recognition test (NORT). The apparatus consisted of a round arena (diameter: 50 cm) with white walls and floor. The box and objects were cleaned between trials to stop the build-up of olfactory cues. Animals received two sessions of 10 min each in the empty box to habituate them to the apparatus and test room. Twenty-four hours later, each mouse was first placed in the box and exposed to two identical objects for 10 min (sample phase). And then one object was replaced by a new novel one and the mouse was placed back in the box and exposed to the familiar object and to a novel test object for a further 10-min (acquisition phase). The STM was tested 10 min after “sample phase” (10-min retention). The experimenters measured the time spent exploring each object. The recognition index was calculated as the percentage ratio of time spent exploring the novel object over total exploration time during acquisition phase. All the behavior tests were performed by at least two researchers who were blinded to genotype and treatment conditions of the mice.

Acute slice preparation

Under anesthesia with urethane (1.5 g/kg, i.p.) mice were sacrificed for electrophysiological and morphological studies at 7-10 days post-peripheral nerve injury. Either hippocampus or lumbar segments (L4-L6) of spinal cord was isolated. Coronal

hippocampal slices (300 μm) or parasagittal spinal cord slices (500 μm) were cut using a vibratome (D.S.K DTK-1000) and superfused with an ice-cold dissection solution containing (in mM): 125 NaCl, 2.5 KCl, 1 $CaCl_2$, 6 $MgCl_2$, 26 $NaHCO_3$, 1.2 NaH_2PO_4, and 25 D-glucose. Then slices were incubated in recording solution containing (in mM): 125 NaCl, 2.5 KCl, 2 $CaCl_2$, 1.2 $MgCl_2$, 26 $NaHCO_3$, 1.2 NaH_2PO_4, and 25 D-glucose for 1h at 34°C before transferring to the recording chamber. Both dissection and recording solutions were saturated with 95% O_2 and 5% CO_2. The hippocampal and spinal slices were recovered for 1h at 34°C before recording or incubation of tetramethylrhodamine-conjugated substance P (TMR-SP, 20 nM) at room temperature.

Organotypic slice culture

Sprague Dawley rats (8-10 old) were rapidly sacrificed under anesthesia with urethane (1.5 g/kg, i.p.) and the brains or L4-L6 segments of spinal cord were dissected. Under aseptic conditions, 400 μm coronal hippocampal slices or transverse spinal cord slices were cut using a vibroslice (WPI NSLM1) in cutting solution (Earle's balance salt solution, 25 mM HEPES) and collected in sterile culture medium containing 50% MEM, 25% heat inactivated horse serum, 25% EBSS, 6.5 mg/ml D-Glucose, 50 U/ml penicillin, 50 μg /ml streptomycin, pH 7.3. The organotypic slices were carefully placed into a 0.4 μm membrane insert (Millipore PICM03050) within a 6-well plate at 37°C and 5% CO_2 with 1 ml culture medium each well. Slices were incubated for at least 6 days before experiments and the medium was changed twice a week. For electrophysiological recording, culture slices were incubated in recording solution containing (in mM): 125

NaCl, 2.5 KCl, 2 $CaCl_2$, 1.2 $MgCl_2$, 26 $NaHCO_3$, 1.2 NaH_2PO_4, and 25 D-glucose for 1h at 34°C before transfer to the recording chamber.

Conditional ablation of microglia

Microglia were selectively killed using a method described previously in which mice genetically engineered to express the diphtheria toxin receptor only in microglia ($CXCR1^{CreER/+}$ mice) were treated with diphtheria toxin (Parkhurst et al., 2013; Peng et al., 2016). Briefly, $CX3CR1^{CreER/+}$ (control) mice or $CX3CR1^{CreER/+}$: $R26^{iDTR/+}$ (M-Abl) mice (over 6 weeks old) were given both tamoxifen (TM) and diphtheria toxin (DT). TM (Sigma T5648, 150 mg/kg, 20 mg/ml in corn oil with ultrasound) was intraperitoneally (i.p.) injected every other day from 10 days before surgery. DT (Sigma C8267, 50 µg/kg, 2.5 µg/ml in PBS) was given for twice at the day before and after surgery (4 days after last TM treatment). To confirm the effectiveness of general microglial ablation in central nervous system, the hippocampus and spinal cord were harvested at 3rd day after surgery to do immunostaining of microglia.

Electrophysiology

Whole-cell recordings were performed at room temperature using an EPC-9 amplifier with Pulse v8.65 software (HEKA Elek., Lambrecht, Germany). For visualizing recorded neurons under microscope (Eclipse FN1, Nikon) infrared DIC optics (IR1000, DAGE-MTI) was used for recording in hippocampal slices. TMR-SP-positive neurons in spinal cord slices were identified under epifluorescence using a CCD camera. The excitatory postsynaptic currents (EPSCs) in hippocampal CA1 pyramidal neurons were

recorded following electrical stimulation of Schaffer collateral-commissural pathway at 0.066 Hz with a bipolar tungsten stimulating electrode. The EPSCs in spinal TMR-SP-positive neurons were evoked by stimulation of the dorsal root entry zone at 0.066 Hz at intensities sufficient to activate C-fibers (0.5ms, 200-500 μA); only the EPSCs evoked by the high intensities were used for further analysis (Nakatsuka et al., 2000). The extracellular solution contained picrotoxin (100 μM, Sigma) to block fast GABAergic inhibition. The recording pipettes (3–5 MΩ) were filled with solution containing (mM): 130 Cs-gluconate, 4 NaCl, 0.5 $MgCl_2$, 5 EGTA, 10 HEPES, 5 MgATP, 0.5 Na_3GTP, 5 QX-314 and 1.3 biocytin (pH 7.3 and osm. 290-295). The AMPAR- and NMDAR-mediated components were distinguished by their differential activation and inactivation kinetics. EPSCs were recorded at different membrane potentials from -70 to +50 mV (10-mV per step). N-methyl-D-aspartate (NMDA) / α-amino-3-hydroxy-5-methyl- 4-isoxazolepropionic acid (AMPA) current ratio NMDA/AMPA ratio is defined as the amplitude of the NMDAR component 80 ms after stimulation at +50 mV divided by the peak of the AMPAR component at -70 mV. Miniature excitatory postsynaptic currents (mEPSCs) were recorded at -70 mV, in the presence of picrotoxin (100 μM) and tetrodotoxin (0.5 μM) in the same recording solution and using same intracellular solution above. mEPSCs were analyzed using the pClamp 9 (Axon Instruments). All the detected events were re-examined and accepted or rejected on the basis of visual examination. Cells were recorded from for roughly 5 min to obtain at least 100 events per cell. Data obtained from the indicated number (n) of cells were expressed as the mean ± s.e.m. and analyzed using Student's *t*-test.

Visualization of neurons and morphological analysis

To visualize recorded neurons, an intracellular marker biocytin (1.3 mM) was dissolved in the intracellular solution/pipette solution described above. After least 15 min whole-cell patch recording, the slices were fixed with 4% paraformaldehyde in PBS and then processed using Alexa Fluor® 594 Streptavidin (Life Technologies) for visualization. Neuronal dendrites and dendritic spines were imaged by confocal microscope (Zeiss LSM 710) through 20X and 63X objectives, respectively. The images were digitally reconstructed and the sum lengths and number of branch points of dendrite were automatically analyzed with Imaris (Bitplane scientific software, RRID:SCR_007370). This study focused on the hippocampal CA1 pyramidal neurons and on the neurokinin-1-positive neurons (NK1-PNs) in spinal lamina I, which is critical for the development of neuropathic pain (Mantyh et al., 1997). The hippocampal CA1 pyramidal neurons were identified by their location within the CA1 cell body layer and by their classic pyramidal shaped soma, apical dendrites and basal dendrites. Spinal NK1-PNs were identified by incubation of spinal cord slices with tetramethylrhodamine-conjugated substance P with red fluorescence that binds to the NK-1 receptor, and therefore labels NK1-PNs (Pagliardini et al., 2005). It has been shown that ~ 80% of lamina I neurons express NK-1 receptor and virtually all (99%) of the NK-1 receptor expressing neurons with soma areas >200 μm^2 are projection neurons (Al Ghamdi et al., 2009). Accordingly, only the NK1-PNs with soma areas >200 μm^2 were recorded from in the present study. The Sholl analysis of neuronal dendrites was also performed with Imaris to provide a quantitative description of the dendritic tree by evaluating the number of dendrites that crossed through virtual concentric circles at equal

distances, centered in the soma of a neuron. The number of spines was manually counted in Imaris, which can show clear spine and three-dimensional actual length, according to a previous work. For each hippocampal CA1 pyramidal neuron, the spines in the principal apical dendrite were counted in a 50 μm to 100 μm segment, which was at least 50 μm away from the center of the soma, and a 30 μm segment of secondary apical dendrite. The spines in basal dendrite were counted in two 15 μm segments, which were at least 20 μm from the soma. For each neurokinin-1-positive neuron in lamina I in spinal cord, spine counting was performed on four 20 μm to 50 μm segments of the dendrite (the proximal end of this segment was never closer than 50 μm from the center of the soma). Spines were counted only if they had both a punctuate head and visible neck. A subset of neurons was counted by two different investigators to ensure consistency of counting. No significant differences were found when the same segment was counted by different investigators.

Western blot

Frozen tissues of hippocampus and spinal dorsal horn were homogenized and equal amounts of proteins were resolved on polyacrylamide gel, and then transferred to PVDF membranes (BD). Membranes were blocked and then probed with primary antibodies: mouse anti- TNF-α (AF-410, R&D System), rabbit anti-BDNF (AB1534, Millipore), mouse anti-β-actin (#3700, Cell Signaling Technology) overnight at 4°C. Membranes were then incubated with an HRP-conjugated secondary antibody (CST) at room temperature. Protein bands were detected by ECL detection reagent (RPN2232; GE Healthcare) and captured on an autoradiography film (Kodak). Integrated optical density

was determined using Image-Pro Plus software 6.0 (Media Cybernetics). Standard curves were constructed to establish that we operated within the linear range of the detection method.

Immunohistochemistry

Mice were deeply anesthetized with isoflurane (5% in O_2) and perfused transcardially with 20 ml PBS followed by 20 ml of cold 4% paraformaldehyde (PFA) in PBS containing 1.5% picric acid. The brain and spinal cord were removed and post-fixed with the same 4% PFA for overnight (brain) or 4-6 hours (spinal cord) at 4 ℃. The samples were then transferred to 30% sucrose in PBS overnight. Sample sections (14 μm in thickness) were prepared on gelatin-coated glass slide with a cryostat (Leica). The sections were blocked with 5% goat serum and 0.3% Triton X-100 (Sigma) in TBS buffer for 60 min, and then incubated overnight at 4℃ with primary antibody for rabbit-anti-Iba1 (1:1000, Wako). The sections were then incubated for 60 min at RT with secondary antibodies (goat anti-rabbit Alexa Fluor®594, Life Technologies). The stained sections were examined with a Leica DFC350 FX (Leica Camera AG, Solms, Germany) fluorescence microscope and images were captured with a CCD spot camera.

The number of GFP^+ cells or the percentage of GFP^+ area was countered or detected using ImageJ software (National Institutes of Health, Bethesda, MD). To quantify immunoreactivity profiles in the spinal cord and hippocampus, three to five L4–5 spinal cord or hippocampal sections per mouse from 3 mice were randomly selected for each group.

Quantification of microglia

All fluorescence images were captured on an EVOS FL (Thermofisher) imaging station with a 20× objective lens, and the qualitative and quantitative analyses of images were performed in a blinded fashion. The number of GFP^+ cells or the percentage of GFP^+ area within hippocampus CA1 or the medial two thirds of the spinal dorsal horn on the ipsilateral side after SNI were counted/measured using Image J software (National Institutes of Health, Bethesda, MD). When GFP^+ cell number counting, image contrast was adjusted to eliminated background fluorescence, and the same cutoff level was used for all images. For GFP^+ area, the images were digitally converted into a grey scale image before commencing the analysis. Only the GFP^+ cell bodies with Dapi-stained nuclei were included in the analysis. To quantify immunoreactivity profiles, three to five L4–5 spinal cord or hippocampal sections per mouse from 3 mice were randomly selected for each group.

Flow cytometry

At 7 d after SNI, the bilateral hippocampus and lumbar 4-5 spinal dorsal horn were harvested from CX3CR1-EGFP mice and digested using Neural Tissue Dissociation Kits (Miltenyi Biotec) as well as proteolytic enzymes to obtain single-cell suspensions. Then the microglia were isolated from the cell suspensions by discontinuous density gradient centrifugation using 30% isotonic Percoll® (GE Healthcare) and stained with APC anti-mouse/human CD11b Antibody (101212, biolegend) and its isotype control for 45 min. The percentage of CX3CR1-EGFP, CD11b+ microglia were compared between sham and SNI groups (n = 3-4 mice /group). Data acquisition was performed on a flow

cytometer (BD FACSCalibur™; BD Biosciences) and analyzed with FlowJo (TreeStar) software blind to treatment group.

Statistics

The data for the Sholl analysis of dendrite distribution with repeated measures two-way ANOVA, and post hoc tests were used for detailed statistical analysis, as appropriate. The behavioral data were analyzed by one-way repeated measure ANOVA when compared within the group and by two-way ANOVA when compared between groups. The results of others were analyzed with Student's *t*-test. All data are expressed as means ± SEM. Statistical tests were carried out with SPSS 16.0 (SPSS, Somers, NY, USA). $p < 0.05$ was considered significant.

Results

SNI oppositely regulates structural synaptic connectivity in the hippocampus and in spinal dorsal horn

This study focused on the neurokinin-1-positive neurons (NK1-PNs) in spinal lamina I, which is critical for the development of neuropathic pain (Mantyh et al., 1997), and on the hippocampal CA1 pyramidal neurons. There are three types of lamina I neurons based on cell morphology, fusiform, multipolar and pyramidal. In the present study, the lamina I NK1-PNs in each group used for morphological analysis included 53%±0.053 fusiform, 42%±0.068 multipolar and 5%±0.037 pyramidal cells. This is consistent with previous studies in rats (Yu et al., 2005) and monkeys (Yu et al., 1999) showing that NK-1 receptors are expressed mainly in fusiform and multipolar, but less in pyramidal lamina I neurons.

Compared with sham-operated mice, the total dendrite length, the number of dendrite branch points and spine densities in the basal and apical dendrites of CA1 pyramidal neurons were significantly reduced (Figure 1A-C), whereas all of these measures of dendritic complexity were enhanced in spinal NK1-PNs (Figure 1D-F) 7-10 d following SNI in mice. Sholl analysis revealed that reduced dendritic branching (number of crossings) in basal dendrites of CA1 neurons was evident between 110 and 140 μm from the soma, in apical dendrites between 230 and 300 μm (Figure1B) and in spinal NK1-positive PNs between 70 to 90 μm (Figure 1E) in SNI mice, compared to sham mice. The results indicate that SNI affects structural synaptic connectivity in a region-dependent manner As most excitatory synapses are located in spines (Sorra and Harris, 2000), these results demonstrated that the number of excitatory synapses is

reduced in hippocampal pyramidal neurons, but enhanced in spinal NK1-PNs under neuropathic pain conditions.

Synaptic efficacy is decreased in the hippocampus but increased in spinal dorsal horn following SNI

Having shown that SNI increases dendritic complexity and spine density in spinal NK1-PNS, but decreases dendritic complexity and spine density in hippocampal CA1 neurons, we next tested if the structural changes were associated with changes in synaptic connectivity in the two regions 7-10 days after SNI. Indeed, we found that, compared with sham mice, the frequency of miniature excitatory postsynaptic currents (mEPSCs) was lower in CA1 pyramidal neurons but was higher in spinal NK1-PNs in SNI mice (Figure 2A-B). The amplitudes of mEPSCs in both CA1 pyramidal neurons and spinal NK1-PNs were not different between SNI and sham groups (Figure 2A-B). The results indicate that the strength of synaptic connectivity is decreased in hippocampal neurons but increased in spinal NK1-PNs, which may result from opposite changes in numbers of excitatory synapses in the two regions in response to SNI.

To investigate if SNI also differentially affects the synaptic plasticity in the two regions, we next tested the effect of SNI on NMDA/AMPA ratio, which reflects the synaptic plasticity (Lau and Zukin, 2007), in the hippocampal and spinal slices with whole-cell patch clamp recordings. We found that the NMDA/AMPA ratio was significantly lower at CA3-CA1 synapses (Figure 2C), but was higher at synapses between primary afferents and spinal NK1-PNs (Figure 2D) in SNI mice, compared to sham mice. These suggest that the synaptic plasticity is decreased in hippocampus but

increased in dorsal horn following peripheral nerve injury, which is in consistence with previous works showing that SNI impairs LTP in hippocampus (Ren et al., 2011) but facilities LTP in spinal dorsal horn (Liu et al., 2007).

The morphological and electrophysiological data demonstrated that SNI induced opposite changes in structural synaptic connectivity, in excitatory synaptic transmission and in synaptic plasticity in hippocampus and in spinal dorsal horn. The following experiments were focused on the mechanisms by which SNI produces the structural synaptic changes and behavioral abnormalities.

The effects of SNI on the expression of TNF-α and BDNF in hippocampus and in spinal dorsal horn

Previous studies showed that elevation of TNF-α is involved in both chronic neuropathic pain (Xu et al., 2006) and memory deficits (Ren et al., 2011) following peripheral nerve injury. BDNF, which is critical for synapse formation, plays important roles in hippocampus-dependent memory (Park and Poo, 2013) and chronic pain (Groth and Aanonsen, 2002; Zhou et al., 2010). To explore the molecules that may contribute to the opposite changes in the dendritic structural and synaptic connectivity changes occurring in SNI, we measured TNF-α and BDNF protein levels in the hippocampus and spinal dorsal horn 7-10 d following SNI. TNF-α levels increased in bilateral hippocampus and in ipsilateral spinal dorsal horn, while BDNF protein decreased in both hippocampi, but increased in the ipsilateral spinal dorsal horn, compared to sham groups (Figure 3A and 3B). These results suggest that overproduction of TNF-α may differentially regulate BDNF expression in hippocampus and spinal dorsal horn.

SNI-induced changes in synaptic connectivity are mediated by TNF-α/TNFR 1 signaling

To determine the role of TNF-α for the changes in structural synaptic change and BDNF expression induced by SNI, we performed experiments with TNF receptor 1 (TNFR1) knock out (KO) mice. There was no difference in the total dendrite lengths, the number of dendrite branch points and spine densities in CA1 pyramidal neurons (Figure 4A-C) and in spinal NK1-PNs (Figure 4D-F) in SNI compared to sham groups of TNFR1 KO mice. Interestingly, just like the changes in synaptic connectivity described above, the opposite regulation of BDNF expression by SNI was also prevented by genetic deletion of TNFR1 (Figure 3G). Thus, TNFR1 may be necessary for the morphological synaptic changes induced by SNI.

To test if TNF-α is sufficient to induce the differential changes in structural synaptic connectivity and BDNF expression in hippocampus and in spinal dorsal horn, we cultured rat hippocampal and spinal cord slices with recombinant rat TNF-α (rrTNF-α) at different concentrations (Figure 5). A rrTNF-α concentration of 10 ng/ml reduced the basal dendrite lengths and the number of basal dendrite branch points in CA1 pyramidal neurons, while the apical dendritic length, apical branch number and both basal and apical spine densities were significantly reduced with 1 ng/ml and 10 ng/ml rrTNF-α (Figure 5A-C). In spinal NK1-PNs, rrTNF-α concentrations of 1 and 10 ng/ml significantly increased total dendrite lengths and the number of dendrite branch points, and dendritic spine density was significantly increased with 10 ng/ml rrTNF-α (Figure 5D-F). Furthermore, rrTNF-α at concentrations of 1 and 10 ng/ml significantly

down-regulated BDNF in hippocampal slices, but up-regulated BDNF in spinal slices (Figure 5G). Thus, TNF-α/TNFR1 signaling may be sufficient to induce CNS region-dependent changes in both synaptic connectivity and BDNF expression under neuropathic pain conditions.

The region-dependent synaptic alterations and BDNF expression induced by SNI are abolished by inhibition or ablation of microglia

We pursued the mechanism by which SNI and resultant elevation of TNF-α oppositely regulate BDNF expression and synaptic connectivity in the spinal dorsal horn and hippocampus. Previous studies showed that activation of microglia impairs LTP in hippocampus (Griffin et al., 2006) but is essential for LTP induction in spinal dorsal horn (Zhong et al., 2010), indicating that microglia have differential effects on synaptic plasticity in the two regions. In the present study, we found that microglia were activated and proliferated in ipsilateral spinal dorsal horn and bilateral hippocampus following SNI in the mice that express GFP in microglial cells (Figure 6A and B). To determine whether microglial activation is responsible for the opposite cellular and molecular changes induced by SNI, we first inhibited microglia using a tetracycline derivative, minocycline. Injection of minocycline (i. p.) prevented memory deficits and mechanical allodynia (Figure 6C), and abolished the upregulation of TNF-α and the opposite changes in BDNF expression (Figure 6D) in the hippocampus and in spinal dorsal horn produced by SNI in wild type mice.

To determine whether microglia mediated the SNI-induced CNS region-dependent changes in synaptic connectivity and BDNF expression, as well as behavioral abnormities,

we selectively ablated microglia using a mouse line genetically engineered to express the diphtheria toxin receptor in microglia in CNS (Parkhurst et al., 2013; Peng et al., 2016). Exposure to diphtheria toxin resulted in extensive depletion of microglia throughout the CNS, including the hippocampus and spinal cord (M-Abl, Figure 7A and B). We found that microglial depletion prevented SNI-induced reductions of dendrite complexity, spine density and the synaptic NMDA/AMPA ratio in hippocampal CA1 pyramidal neurons (Figure 7C and D), and the increases in those dendritic features in spinal dorsal horn NK1-PNs (Figure 7E and F). Finally, the ablation of microglia also prevented the SNI-induced short-term memory deficits and mechanical allodynia (Figure 7G) and abolished the increase in TNF-α and the differential changes in BDNF in the hippocampus and spinal dorsal horn (Figure 7H). These results suggest a pivotal role for microglial activation in the neurochemical and cytoarchitectural consequences of SNI in the spinal dorsal horn and hippocampus, and the associated behavioral manifestations.

Discussion

We found that dendritic structural complexity and functional synaptic connectivity and BDNF expression were significantly enhanced in spinal NK1-PNs but reduced in hippocampal CA1 neurons following SNI. SNI upregulated TNF-α in both hippocampus and spinal dorsal horn and the SNI-induced region-dependent changes in structural synaptic connectivity and BDNF expression were blocked by genetic deletion of TNFR1 *in vivo*, mimicked by rrTNF-α in cultured hippocampal and spinal slices. SNI also activated microglia in the two regions while the pharmacological inhibition or selective deletion of microglia blocked the SNI-induced changes in synaptic connectivity and

BDNF expression and substantially prevented the neuropathic pain and short-term memory deficits. Altogether, our findings suggest that CNS region-dependent changes in synaptic connectivity are responsible for behavioral manifestations of chronic pain including impaired hippocampus-dependent learning and memory. Microglial activation and TNF-α signaling via TNFR1 are required for the opposite changes in the structural synaptic connectivity in region CA1 of the hippocampus and spinal cord dorsal horn.

The CNS region-specific effects of SNI on synaptic connectivity are mediated by microglial activation and TNF-α signaling.

Previous studies showed that activation of microglia impairs LTP in hippocampus (Griffin et al., 2006) but is essential for LTP induction in spinal dorsal horn (Zhong et al., 2010), indicating that microglial activation also affect synaptic plasticity in a region-dependent manner. Microglia release numerous gliotransmitters, including cytokines, neurotrophic factors and neurotransmitters (Ransohoff and Perry, 2009; Eyo and Wu, 2013) and these chemical substances may create and maintain a microenvironment that modulates the structure and function of the cells. Under neuropathic pain conditions, it is well known that spinal microglia are strongly activated at both molecular and cellular level, thereby regulating neuronal activities in the spinal dorsal horn (Zhuo et al., 2011; Gu et al., 2016; Jeong et al., 2016). However, the peripheral nerve injury-induced microglia activation in the brain is less conclusive. For example, a previous study showed that ligation of common peroneal nerve fails to activate cortical or hippocampal microglia (Zhang et al., 2008), which is different from the current study. We believe that the different pain models used in the studies may

underlie the discrepancy. Indeed, Takeda (Takeda et al., 2009) reported that the expression of CD11b, a microglial marker, was increased in the hypothalamus and periaqueductal gray in the chronic constriction injury rats. In addition, it has been shown that peripheral inflammation induces microglia activation in the hippocampus (Riazi et al., 2008). A recent genome-wide analysis study shows that microglia have distinct brain region-dependent transcriptional identities (Grabert et al., 2016). Accordingly, the gliotransmitters released by activated microglia in hippocampus and in spinal dorsal horn may be different under neuropathic pain conditions. If this is true, the opposite changes in the synaptic connectivity in the two regions may result from the different microenvironment mediated by microglia. Indeed, our data showing that SNI-induced opposite changes in synaptic connectivity and BDNF expression were prevented by either pharmacological inhibition or genetic ablation of microglia demonstrate directly that the region-dependent changes induced by SNI are mediated by microglial activation.

Similar to peripheral nerve injury and microglial activation, TNF-α overproduction also regulates synaptic plasticity region-dependently: induction of LTP in the spinal dorsal horn (Liu et al., 2007; Zhong et al., 2010; Gruber-Schoffnegger et al., 2013) and inhibition of LTP in the hippocampus (Pickering et al., 2005; Griffin et al., 2006; Ren et al., 2011). The present work showed that SNI-induced opposite changes in structural synaptic connectivity hippocampus and in spinal dorsal horn were abolished by genetic deletion of TNFR1 and mimicked by rrTNF-α in slice cultures. The mechanisms underlying the effects of TNF-α/ TNFR1 signaling are still unclear. In neuropathic conditions TNF-α released from neurons and glial cells (Xu et al., 2006) can activate

microglia via TNFR1 *in vivo* (Ishikawa et al., 2013) and *in vitro* (Neniskyte et al., 2014). Therefore, TNF-α-induced CNS region-dependent changes may be at least partially mediated by microglia TNFR1.

BDNF in SNI-induced structural and synaptic plasticity in the hippocampus and spinal dorsal horn

It is well established that LTP and learning are associated with increases in dendritic spines in hippocampal and cortical neurons (Holtmaat and Svoboda, 2009) and the structural plasticity is believed to underlie long-term memory formation (Bailey and Kandel, 1993). The change in spine number is associated with functional changes in synaptic connectivity and behavioral changes. For example, animal studies have shown that exercise and caloric restriction increase dendritic spine density in hippocampal neurons and improve learning and memory, whereas diabetes and depression reduce spine density and impair learning and memory (Stranahan et al., 2009; Mattson, 2012). Previous findings show that peripheral nerve injury that leads to neuropathic pain (Decosterd and Woolf, 2000) and short-term memory induces LTP at C-fiber synapses in spinal dorsal horn (Zhang et al., 2004) but inhibits LTP at CA3-CA1 synapses in hippocampus (Ren et al., 2011). We found that total dendrite length, the number of dendrite branch points and spine densities were reduced in CA1 pyramidal neurons but enhanced in spinal NK1-PNs 7-10d after SNI. As most excitatory synapses are located in spines (Sorra and Harris, 2000), the opposite structural synaptic changes may contribute to long-lasting memory deficits and chronic neuropathic pain by decreasing and increasing excitatory synaptic transmission in hippocampus and in spinal dorsal horn,

545 respectively. The reduction of the dendritic complexity in hippocampus may also
546 contribute to the hippocampal atrophy in chronic pain patients (Mutso et al., 2012; Mao
547 et al., 2016).

548 BDNF is critical for dendritic growth, synapse formation and functional synaptic
549 plasticity in several CNS regions including the hippocampus and spinal dorsal horn
550 (Coull et al., 2005; Zhou et al., 2010). We found that BDNF levels were reduced in
551 hippocampus but increased in spinal dorsal horn following SNI, and that these changes in
552 BDNF were mediated by microglia activation and TNFR1. These findings are consistent
553 with a scenario in which microglia-derived TNF-α differentially regulates BDNF
554 expression in hippocampal CA1 and spinal dorsal horn neurons. Given that BDNF is
555 known to stimulate dendrite growth and synaptogenesis in both CNS regions (Lu et al.,
556 2013), it seems likely that changes in BDNF expression contribute to the differential
557 effects of SNI on dendritic architecture and synaptic connectivity in hippocampal CA1
558 pyramidal neurons and spinal NK-1 receptor-expressing neurons.

559 Altogether, our study demonstrates a differential regulation of synaptic plasticity in the
560 hippocampus and spinal cord by a TNFα- and microglia-dependent mechanism after
561 peripheral nerve injury. These findings suggest that suppression of microglial activation
562 or inhibition of TNFR1 might ameliorate the adverse effects of chronic pain on mood and
563 learning and memory. They may also explain, in part, the fact that exercise is beneficial
564 for chronic pain patients because it reduces pain perception and also exhibits
565 antidepressant and cognition-enhancing effects (Ambrose and Golightly, 2015).
566 Interestingly, exercise increased BDNF expression in the hippocampus, but suppresses

BDNF production in the spinal dorsal horn (Mattson, 2012; Almeida et al., 2015). It will be of considerable interest to determine whether there are roles for microglia and TNF-α in these beneficial effects of exercise on chronic pain.

Reference

Al Ghamdi KS, Polgar E, Todd AJ (2009) Soma size distinguishes projection neurons from neurokinin 1 receptor-expressing interneurons in lamina I of the rat lumbar spinal dorsal horn. Neuroscience 164:1794-1804.

Almeida C, DeMaman A, Kusuda R, Cadetti F, Ravanelli MI, Queiroz AL, Sousa TA, Zanon S, Silveira LR, Lucas G (2015) Exercise therapy normalizes BDNF upregulation and glial hyperactivity in a mouse model of neuropathic pain. Pain 156:504-513.

Ambrose KR, Golightly YM (2015) Physical exercise as non-pharmacological treatment of chronic pain: Why and when. Best practice & research Clinical rheumatology 29:120-130.

Awh E, Vogel EK, Oh SH (2006) Interactions between attention and working memory. Neuroscience 139:201-208.

Bailey CH, Kandel ER (1993) Structural changes accompanying memory storage. Annual review of physiology 55:397-426.

Coull JA, Beggs S, Boudreau D, Boivin D, Tsuda M, Inoue K, Gravel C, Salter MW, De Koninck Y (2005) BDNF from microglia causes the shift in neuronal anion gradient underlying neuropathic pain. Nature 438:1017-1021.

Decosterd I, Woolf CJ (2000) Spared nerve injury: an animal model of persistent peripheral neuropathic pain. Pain 87:149-158.

Dick BD, Rashiq S (2007) Disruption of Attention and Working Memory Traces in Individuals with Chronic Pain. Anesthesia Analgesia 104:1223-1229.

Eccleston C (1995) Chronic pain and distraction: An experimental investigation into the role of sustained and shifting attention in the processing of chronic persistent pain. Behaviour Research and Therapy 33:391-405.

Eyo UB, Wu LJ (2013) Bidirectional microglia-neuron communication in the healthy brain. Neural plasticity 2013:456857.

Grabert K, Michoel T, Karavolos MH, Clohisey S, Baillie JK, Stevens MP, Freeman TC, Summers KM, McColl BW (2016) Microglial brain region-dependent diversity and selective regional sensitivities to aging. Nat Neurosci.

Griffin R, Nally R, Nolan Y, McCartney Y, Linden J, Lynch MA (2006) The age-related attenuation in long-term potentiation is associated with microglial activation. Journal of Neurochemistry 99:1263-1272.

Groth R, Aanonsen L (2002) Spinal brain-derived neurotrophic factor (BDNF) produces hyperalgesia in normal mice while antisense directed against either BDNF or trkB, prevent inflammation-induced hyperalgesia. Pain 100:171-181.

Gruber-Schoffnegger D, Drdla-Schutting R, Honigsperger C, Wunderbaldinger G, Gassner M, Sandkuhler J (2013) Induction of thermal hyperalgesia and synaptic long-term potentiation in the spinal cord lamina I by TNF-alpha and IL-1beta is mediated by glial cells. J Neurosci 33:6540-6551.

611 Gu N, Peng J, Murugan M, Wang X, Eyo UB, Sun D, Ren Y, DiCicco-Bloom E, Young
612 W, Dong H, Wu LJ (2016) Spinal Microgliosis Due to Resident Microglial
613 Proliferation Is Required for Pain Hypersensitivity after Peripheral Nerve Injury.
614 Cell reports 16:605-614.
615 Hart RP, Martelli MF, Zasler ND (2000) Chronic pain and neuropsychological
616 functioning. NeuropsycholRev 10:131-149.
617 Holtmaat A, Svoboda K (2009) Experience-dependent structural synaptic plasticity in the
618 mammalian brain. Nat Rev Neurosci 10:647-658.
619 Ishikawa T, Miyagi M, Kamoda H, Orita S, Eguchi Y, Arai G, Suzuki M, Sakuma Y,
620 Oikawa Y, Inoue G, Aoki Y, Toyone T, Takahashi K, Ohtori S (2013) Differences
621 between tumor necrosis factor-alpha receptors types 1 and 2 in the modulation of
622 spinal glial cell activation and mechanical allodynia in a rat sciatic nerve injury
623 model. Spine 38:11-16.
624 Jeong H, Na YJ, Lee K, Kim YH, Lee Y, Kang M, Jiang BC, Yeom YI, Wu LJ, Gao YJ,
625 Kim J, Oh SB (2016) High-resolution transcriptome analysis reveals neuropathic
626 pain gene-expression signatures in spinal microglia after nerve injury. Pain
627 157:964-976.
628 Ji RR, Suter MR (2007) p38 MAPK, microglial signaling, and neuropathic pain. MolPain
629 3:33.
630 Lau CG, Zukin RS (2007) NMDA receptor trafficking in synaptic plasticity and
631 neuropsychiatric disorders. Nature reviews Neuroscience 8:413-426.
632 Liu YL, Zhou LJ, Hu NW, Xu JT, Wu CY, Zhang T, Li YY, Liu XG (2007) Tumor
633 necrosis factor-alpha induces long-term potentiation of C-fiber evoked field
634 potentials in spinal dorsal horn in rats with nerve injury: the role of NF-kappa B,
635 JNK and p38 MAPK. Neuropharmacology 52:708-715.
636 Lu B, Nagappan G, Guan X, Nathan PJ, Wren P (2013) BDNF-based synaptic repair as a
637 disease-modifying strategy for neurodegenerative diseases. Nature reviews
638 Neuroscience 14:401-416.
639 Mantyh PW, Rogers SD, Honore P, Allen BJ, Ghilardi JR, Li J, Daughters RS, Lappi DA,
640 Wiley RG, Simone DA (1997) Inhibition of hyperalgesia by ablation of lamina I
641 spinal neurons expressing the substance P receptor. Science 278:275-279.
642 Mao CP, Bai ZL, Zhang XN, Zhang QJ, Zhang L (2016) Abnormal Subcortical Brain
643 Morphology in Patients with Knee Osteoarthritis: A Cross-sectional Study.
644 Frontiers in aging neuroscience 8:3.
645 Mattson MP (2012) Energy intake and exercise as determinants of brain health and
646 vulnerability to injury and disease. Cell metabolism 16:706-722.
647 Mutso AA, Radzicki D, Baliki MN, Huang L, Banisadr G, Centeno MV, Radulovic J,
648 Martina M, Miller RJ, Apkarian AV (2012) Abnormalities in hippocampal
649 functioning with persistent pain. The Journal of neuroscience : the official journal
650 of the Society for Neuroscience 32:5747-5756.
651 Nakatsuka T, Ataka T, Kumamoto E, Tamaki T, Yoshimura M (2000) Alteration in

synaptic inputs through C-afferent fibers to substantia gelatinosa neurons of the rat spinal dorsal horn during postnatal development. Neuroscience 99:549-556.

Neniskyte U, Vilalta A, Brown GC (2014) Tumour necrosis factor alpha-induced neuronal loss is mediated by microglial phagocytosis. FEBS letters 588:2952-2956.

Pagliardini S, Adachi T, Ren J, Funk GD, Greer JJ (2005) Fluorescent tagging of rhythmically active respiratory neurons within the pre-Botzinger complex of rat medullary slice preparations. J Neurosci 25:2591-2596.

Park H, Poo MM (2013) Neurotrophin regulation of neural circuit development and function. Nat Rev Neurosci 14:7-23.

Parkhurst CN, Yang G, Ninan I, Savas JN, Yates JR, 3rd, Lafaille JJ, Hempstead BL, Littman DR, Gan WB (2013) Microglia promote learning-dependent synapse formation through brain-derived neurotrophic factor. Cell 155:1596-1609.

Peng J, Gu N, Zhou L, U BE, Murugan M, Gan WB, Wu LJ (2016) Microglia and monocytes synergistically promote the transition from acute to chronic pain after nerve injury. Nature communications 7:12029.

Pickering M, Cumiskey D, O'Connor JJ (2005) Actions of TNF-alpha on glutamatergic synaptic transmission in the central nervous system. ExpPhysiol 90:663-670.

Ransohoff RM, Perry VH (2009) Microglial physiology: unique stimuli, specialized responses. Annual review of immunology 27:119-145.

Ren WJ, Liu Y, Zhou LJ, Li W, Zhong Y, Pang RP, Xin WJ, Wei XH, Wang J, Zhu HQ, Wu CY, Qin ZH, Liu G, Liu XG (2011) Peripheral nerve injury leads to working memory deficits and dysfunction of the hippocampus by upregulation of TNF-alpha in rodents. Neuropsychopharmacology : official publication of the American College of Neuropsychopharmacology 36:979-992.

Riazi K, Galic MA, Kuzmiski JB, Ho W, Sharkey KA, Pittman QJ (2008) Microglial activation and TNFalpha production mediate altered CNS excitability following peripheral inflammation. Proceedings of the National Academy of Sciences of the United States of America 105:17151-17156.

Rowan MJ, Klyubin I, Wang Q, Hu NW, Anwyl R (2007) Synaptic memory mechanisms: Alzheimer's disease amyloid beta-peptide-induced dysfunction. BiochemSocTrans 35:1219-1223.

Sorra KE, Harris KM (2000) Overview on the structure, composition, function, development, and plasticity of hippocampal dendritic spines. Hippocampus 10:501-511.

Stranahan AM, Lee K, Martin B, Maudsley S, Golden E, Cutler RG, Mattson MP (2009) Voluntary exercise and caloric restriction enhance hippocampal dendritic spine density and BDNF levels in diabetic mice. Hippocampus 19:951-961.

Takeda K, Muramatsu M, Chikuma T, Kato T (2009) Effect of memantine on the levels of neuropeptides and microglial cells in the brain regions of rats with neuropathic pain. J Mol Neurosci 39:380-390.

693 Wu Y, Na X, Zang Y, Cui Y, Xin W, Pang R, Zhou L, Wei X, Li Y, Liu XG (2014)
694 Upregulation of tumor necrosis factor-alpha in nucleus accumbens attenuates
695 morphine-induced rewarding in a neuropathic pain model. Biochemical and
696 biophysical research communications 449:502-507.
697 Xu JT, Xin WJ, Zang Y, Wu CY, Liu XG (2006) The role of tumor necrosis factor-alpha
698 in the neuropathic pain induced by Lumbar 5 ventral root transection in rat. Pain
699 123:306-321.
700 Zhang F, Vadakkan KI, Kim SS, Wu LJ, Shang Y, Zhuo M (2008) Selective activation of
701 microglia in spinal cord but not higher cortical regions following nerve injury in
702 adult mouse. Molecular pain 4:15.
703 Zhang HM, Zhou LJ, Hu XD, Hu NW, Zhang T, Liu XG (2004) Acute nerve injury
704 induces long-term potentiation of C-fiber evoked field potentials in spinal dorsal
705 horn of intact rat. Sheng Li XueBao 56:591-596.
706 Zhong Y, Zhou LJ, Ren WJ, Xin WJ, Li YY, Zhang T, Liu XG (2010) The direction of
707 synaptic plasticity mediated by C-fibers in spinal dorsal horn is decided by
708 Src-family kinases in microglia: The role of tumor necrosis factor-alpha. Brain
709 BehavImmun 24:874-880.
710 Zhou LJ, Ren WJ, Zhong Y, Yang T, Wei XH, Xin WJ, Liu CC, Zhou LH, Li YY, Liu XG
711 (2010) Limited BDNF contributes to the failure of injury to skin afferents to
712 produce a neuropathic pain condition. Pain 148:148-157.
713 Zhuo M, Wu G, Wu LJ (2011) Neuronal and microglial mechanisms of neuropathic pain.
714 Molecular brain 4:31.
715
716
717

Legends

Figure 1. Synaptic connectivity is decreased in hippocampus but increased in spinal dorsal horn after SNI.

(A, B) Representative images of biocytin-labeled CA1 pyramidal neurons and summary data of dendritic length (n = 12, basal, $p = 0.024$; apical, $p = 0.002$), branch number (n = 12; basal, $p = 0.024$, apical, $p = 0.002$) and Sholl analysis in wild type (WT) from the sham and SNI groups (n=12, $p = 0.012$). **(C)** Representative images and summary data of dendritic spine densities of CA1 neurons in the indicated groups (n = 12, basal, $p = 0.023$; apical, $p = 0.021$). 12 neurons from 6 mice per group were analyzed. **(D, E)** Representative images and the summary data of dendritic length (n = 14, $p = 0.024$), branch number (n = 14, $p = 0.016$) and Sholl analysis of spinal NK1-PNs in sham and SNI groups of WT mice (n=14, $p = 0.014$). **(F)** Representative images and summary data of dendritic spine densities of spinal NK1-PNs in the indicated groups (n = 14, $p = 0.023$). 14 neurons from 6 mice per group. Values are the mean ± SEM. *$p < 0.05$ versus sham groups. Data for all bar graphs were analyzed using Student's t-test. Data for graphs in which Sholl analyses is plotted were analyzed using repeated measures two-way ANOVA.

Figure 2. SNI induces differential changes in synaptic transmission

(**A**) Representative mEPSCs of CA1 pyramidal neurons, their amplitude, cumulative probability and frequency in WT mice from the sham and SNI groups (n = 12, amplitude, $p = 0.659$; frequency, $p = 0.008$; 12 neurons from 6 mice per group). (**B**) Representative mEPSCs of spinal NK1-PNs, their amplitude, cumulative probability and frequency in

WT mice from the sham and SNI groups (n = 10, amplitude, $p = 0.819$; frequency, $p = 0.012$; 10 neurons from 5 mice per group). (**C**) The NMDA/AMPA current ratios at CA3-CA1 synapses in the indicated groups (n = 15, $p = 0.021$; 15 neurons from 6 mice per group). The evoked AMPA receptor EPSC (low traces) and the evoked NMDA receptor EPSC (up traces) were recorded at membrane potentials of -70 and +50 mV, respectively. The circles indicate the time at which the amplitudes of AMPA or NMDA receptor currents were measured. (**D**) The NMDA/AMPA current ratio in spinal NK1-PNs in the different groups (n = 16, $p = 0.022$; 16 neurons from 6 mice per group). Values are the mean ± SEM. *$p < 0.05$, **$p < 0.01$ versus sham groups. Data for all bar graphs were analyzed using Student's t-test.

Figure 3. The effects of SNI on TNF-α and BDNF expression in hippocampus and spinal dorsal horn

(**A**) Western blots show the levels of TNF-α (26 kDa) and BDNF (18 kDa) in contralateral (C) and ipsilateral (I) hippocampus of WT mice in sham and SNI groups (n=5, TNF-α, $p < 0.001$ (I), $p = 0.009$ (C); BDNF, $p < 0.001$ (I), $p = 0.021$ (C)). (**B**) The levels of TNF-α and BDNF in contralateral and ipsilateral spinal dorsal horn in the indicated groups (n=5, TNF-α, $p = 0.014$ (I), $p = 0.662$ (C); BDNF, $p = 0.032$ (I), $p = 0.737$ (C). RelOD: relative optical density. Values are the mean ± SEM. *$p < 0.05$, **$p < 0.01$, ***$p < 0.001$ versus sham groups. Data for all bar graphs were analyzed using Student's t-test.

Figure 4. The effects of SNI on synaptic connectivity and BDNF expression are

764 **prevented by genetic deletion of TNFR 1.**

765 **(A)** Representative images of biocytin-labeled CA1 pyramidal neurons and **(B)** their
766 indicated dendritic length (n = 12, basal, $p = 0.361$; apical, $p = 0.335$), branch number (n
767 = 12, basal, $p = 0.395$; apical, $p = 0.605$) and Sholl analysis (n=12, $p = 0.231$) in TNFR1
768 KO mice from the sham and SNI groups are shown. **(C)** Representative images and
769 summary data of dendritic spine densities of CA1 neurons in the indicated groups (n = 12,
770 basal, $p = 0.406$; apical, $p = 0.369$). 12 neurons from 6 mice per group were used for the
771 morphological analysis. **(D, E)** Representative images and the summary data of dendritic
772 length (n = 14, $p = 0.234$), branch number (n = 14, $p = 0.394$) and Sholl analysis of spinal
773 NK1-PNs in sham and SNI groups of TNFR1 KO mice (n=14, $p = 0.320$). **(F)**
774 Representative images and summary data of dendritic spine densities of spinal NK1-PNs
775 in the indicated groups (n = 14, $p = 0.234$). 14 neurons from 6 mice per group. **(G)**
776 Western blots show the level of BDNF in contralateral (C) and ipsilateral (I)
777 hippocampus or spinal dorsal horn of TNFR1 KO mice in sham and SNI groups
778 (hippocampus, n = 5, $p = 0.422$ (C), $p = 0.485$ (I); spinal dorsal horn, n = 5, $p = 0.298$)
779 (C), $p = 0.372$ (I). Data for all bar graphs were analyzed using Student's t-test. Data for
780 graphs in which Sholl analyses is plotted were analyzed using repeated measures
781 two-way ANOVA.
782
783 **Figure 5. TNF-α differentially modulates synaptic connectivity and BDNF**
784 **expression in cultured slices. (A, B)** Representative images of biocytin-labeled CA1
785 pyramidal neurons and their indicated dendritic length (n = 12, basal, vehicle vs 1 ng, $p =$
786 0.368, vehicle vs 10 ng, $p < 0.001$, 1 ng vs 10 ng, $p = 0.007$; apical, vehicle vs 1 ng, $p =$

0.005, vehicle vs 10 ng, $p = 0.001$, 1 ng vs 10 ng, $p = 0.898$), branch number (n = 12, basal, vehicle vs 1 ng, $p = 0.692$, vehicle vs 10 ng, $p = 0.003$, 1 ng vs 10 ng, $p = 0.013$; apical, vehicle vs 1 ng, $p = 0.044$, vehicle vs 10 ng, $p < 0.001$, 1 ng vs 10 ng, $p = 0.208$) and Sholl analysis (n=14, $p = 0.012$) in the slices treated with vehicle and rrTNF-α (TNF) at indicated concentrations. **(C)** Representative images and summary data show dendritic spine densities in CA1 pyramidal neurons in vehicle- and TNF-treated slices (n = 12, basal, vehicle vs 1 ng, $p < 0.001$, vehicle vs 10 ng, $p < 0.001$, 1 ng vs 10 ng, $p = 0.895$; apical, vehicle vs 1 ng, $p = 0.026$, vehicle vs 10 ng, $p = 0.02$, 1 ng vs 10 ng, $p = 0.914$). 12 neurons in 12 slices from 6 rats per group. **(D, E)** Representative images and dendritic measurements of spinal NK1-PNs in vehicle- and TNF-treated slices (n = 12, dendritic length, vehicle vs 1 ng, $p < 0.001$, vehicle vs 10 ng, $p = 0.001$, 1 ng vs 10 ng, $p = 0.875$; branch number, vehicle vs 1 ng, $p < 0.001$, vehicle vs 10 ng, $p < 0.001$, 1 ng vs 10 ng, $p = 0.126$; Sholl analysis, n=12, $p = 0.022$). **(F)** The dendritic spines of NK1-PNs were increased by TNF (n=12, vehicle vs 1 ng, $p = 0.211$, vehicle vs 10 ng, $p = 0.004$, 1 ng vs 10 ng, $p = 0.218$). 12 neurons in 12 slices from 6 rats per group. **(G)** Western blots show BDNF levels in the hippocampal and spinal slice cultures in the indicated groups (n = 5, vehicle vs 1 ng, $p = 0.035$, vehicle vs 10 ng, $p < 0.001$, 1 ng vs 10 ng, $p = 0.022$). 30-35 slices from 5 rats per group. Values are the mean ± SEM. *$p < 0.05$, **$p < 0.01$, ***$p < 0.001$ versus vehicle; #<0.05, ##<0.01 versus 1 ng/ml. Data for all bar graphs were analyzed using one-way ANOVA. Data for graphs in which Sholl analyses is plotted were analyzed using repeated measures two-way ANOVA

Figure 6. Pharmacological inhibition of microglia prevents the opposite changes in BDNF expression and behavioral abnormalities induced by SNI. (A) Representative

images show microglial cells (green) and Dapi (Blue) in ipsilateral hippocampal CA1 and spinal dorsal horn in CX3CR1-EGFP mice from sham and SNI groups. Pooled results show the number of GFP^+ cells and the percentage of GFP^+ area in the hippocampus (Hip, n = 3, $p = 0.021$) and spinal dorsal horn (SDH, n = 3, $p < 0.001$) of SNI and sham mice 9 d after surgery (3 mice for each group). **(B)** Fluorescence-activated cell sorting (FACS) analysis of microglia in the ipsilateral (ipsi) and contralateral (contr) hippocampus (n = 4, sham vs SNI Ipsi, $p < 0.001$, sham vs SNI Contr, $p < 0.001$) and spinal dorsal horn (n = 4, sham vs SNI Ipsi, $p < 0.001$, sham vs SNI Contr, $p = 0.092$) in sham and SNI-7d mice. Dot plots show the total number of microglial cells expressing CX_3CR1-EGFP and CD11b (4 mice for each group). **(C)** The short-term memory deficit (n = 8, Vehicle +Sham vs Vehicle +SNI, $p = 0.013$, Mino +Sham vs Mino +SNI, $p = 0.142$) and mechanical allodynia (sample size mentioned in figure, day 7, Vehicle +Sham vs Vehicle +SNI, $p < 0.001$, Mino +Sham vs Mino +SNI, $p = 0.362$; day 13, Vehicle +Sham vs Vehicle +SNI, $p < 0.001$, Mino +Sham vs Mino +SNI, $p = 0.566$) were prevented by minocycline (i.p., 30 mg/kg, twice a day beginning one day prior to and continuing for 7 days after SNI). **(D)** Western blots show the expression of TNF-α and BDNF in hippocampus (n = 5, TNF-α, Vehicle +Sham vs Vehicle +SNI, $p < 0.001$, Mino +Sham vs Mino +SNI, $p = 0.361$; BDNF, Vehicle +Sham vs Vehicle +SNI, $p = 0.008$, Mino +Sham vs Mino +SNI, $p = 0.225$) and spinal dorsal horn (n = 5, TNF-α, Vehicle +Sham vs Vehicle +SNI, $p < 0.001$, Mino +Sham vs Mino +SNI, $p = 0.566$; BDNF, Vehicle +Sham vs Vehicle +SNI, $p < 0.001$, Mino +Sham vs Mino +SNI, $p = 0.306$) tissues from the

mice that had been used for the above behavioral tests. Values are the mean ± SEM. *p < 0.05, **p < 0.01, ***p < 0.001 compared to the values for each of the other three groups. Data for bar graphs in panel A were analyzed using Student's t-test. Data for graphs in panel C were analyzed using repeated measures two-way ANOVA. Data for other graphs were analyzed using Student's t-test.

Figure 7. Conditional ablation of microglia prevents the synaptic changes and the behavioral abnormalities resulting from SNI. **(A)** The experimental diagram shows the timeline of drug treatments (TM, tamoxifen, DT, diphtheria toxin), immunostaining, western blots (WB) pain behavioral tests (Pain beha.), novel object recognition test (NORT) and electrophysiology (EP) before and after SNI. (**B**) The photographs show Iba1-positive microglia in the hippocampal CA1 area and spinal dorsal horn of $CX3CR1^{CreER/+}$ (Control) and $CX3CR1^{CreER/+:}R26^{iDTR/+}$ mice (M-Abl) 3 day after SNI. (**C**) Results of analyses of dendritic length (n = 12, basal, Control +Sham vs Control +SNI, p = 0.011, M-Abl +Sham vs M-Abl +SNI, p = 0.568; apical, Control +Sham vs Control +SNI, p = 0.035, M-Abl +Sham vs M-Abl +SNI, p = 0.399), branch number (n = 12, basal, Control +Sham vs Control +SNI, p = 0.013, M-Abl +Sham vs M-Abl +SNI, p = 0.208; apical, Control +Sham vs Control +SNI, p = 0.022, M-Abl +Sham vs M-Abl +SNI, p = 0.451), and spine densities of CA1 neurons in sham and SNI groups of control and M-Abl mice (n = 12, basal, Control +Sham vs Control +SNI, p = 0.039, M-Abl +Sham vs M-Abl +SNI, p = 0.602; apical, Control +Sham vs Control +SNI, p = 0.028, M-Abl

+Sham vs M-Abl +SNI, $p = 0.375$; 12 neurons from 5 mice per group). (**D**) The NMDA/AMPA current ratio at CA3-CA1 synapses in SNI group was lower in control mice but not in M-Abl mice, compared to sham groups (n = 14, Control +Sham vs Control +SNI, $p = 0.022$, M-Abl +Sham vs M-Abl +SNI, $p = 0.412$). **(E)** Results of analyses of dendritic length (n = 12, Control +Sham vs Control +SNI, $p = 0.021$, M-Abl +Sham vs M-Abl +SNI, $p = 0.226$), branch number (n = 12, Control +Sham vs Control +SNI, $p = 0.017$, M-Abl +Sham vs M-Abl +SNI, $p = 0.336$), and spine densities of spinal NK1-PN neurons in sham and SNI groups of control and M-Abl mice (n = 12, Control +Sham vs Control +SNI, $p = 0.014$, M-Abl +Sham vs M-Abl +SNI, $p = 0.433$; 12 neurons from 5 mice per group). **(F)** The NMDA/AMPA current ratio in spinal NK1-PNs in different groups (n = 12, Control +Sham vs Control +SNI, $p = 0.031$, M-Abl +Sham vs M-Abl +SNI, $p = 0.522$). 12 neurons from 5 mice per group. **(G)** The recognition index for short-term memory (n = 10, Control +Sham vs Control +SNI, $p = 0.026$, M-Abl +Sham vs M-Abl +SNI, $p = 0.559$) and mechanical allodynia (sample size mentioned in figure, day 3, Control +Sham vs Control +SNI, $p < 0.001$, M-Abl +Sham vs M-Abl +SNI, $p = 0.306$; day 5, Control +Sham vs Control +SNI, $p < 0.001$, M-Abl +Sham vs M-Abl +SNI, $p = 0.528$; day 7, Control +Sham vs Control +SNI, $p < 0.001$, M-Abl +Sham vs M-Abl +SNI, $p = 0.672$) in sham and SNI groups of control and M-Abl mice. **(H)** The expression of TNF-α and BDNF in hippocampal (n = 5, TNF-α, Control +Sham vs Control +SNI, $p < 0.001$, M-Abl +Sham vs M-Abl +SNI, $p = 0.162$; BDNF, Control +Sham vs Control +SNI, $p = 0.035$, M-Abl +Sham vs M-Abl +SNI, $p = 0.098$) and spinal

dorsal horn (n = 5, TNF-α, Control +Sham vs Control +SNI, $p < 0.001$, M-Abl +Sham vs M-Abl +SNI, $p = 0.377$; BDNF, Control +Sham vs Control +SNI, $p < 0.001$, M-Abl +Sham vs M-Abl +SNI, $p = 0.568$) tissues from the mice that had been used for the above behavioral tests. Values are the mean ± SEM. *$p < 0.05$, **$p < 0.01$, ***$p < 0.001$ compared to the values for each of the other three groups. Data for graphs in panel G were analyzed using repeated measures two-way ANOVA. Data for other graphs were analyzed using Student's t-test.

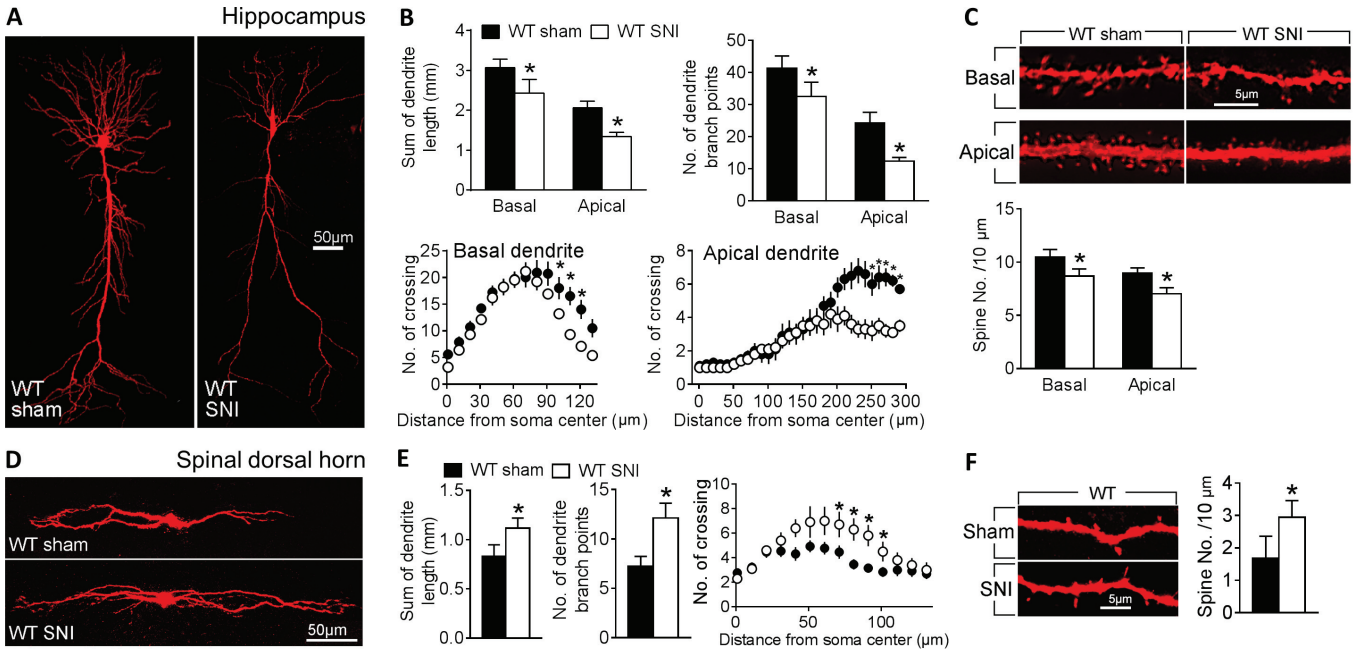

Fig. 1

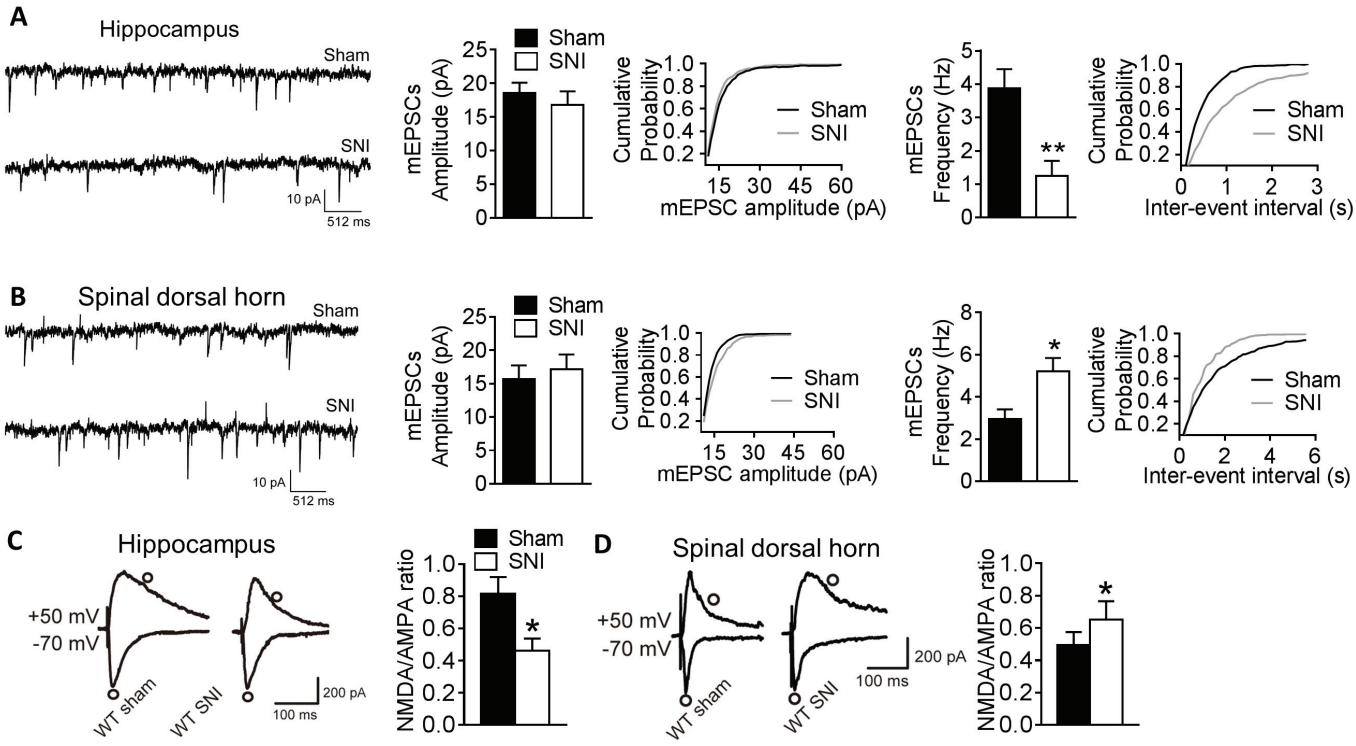

Fig. 2

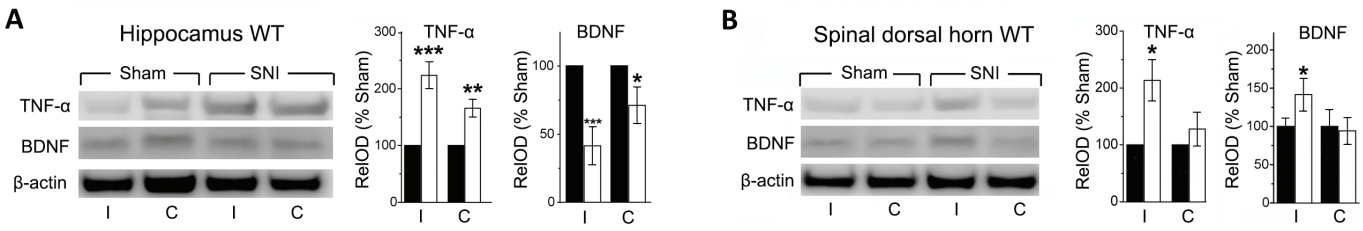

Fig. 3

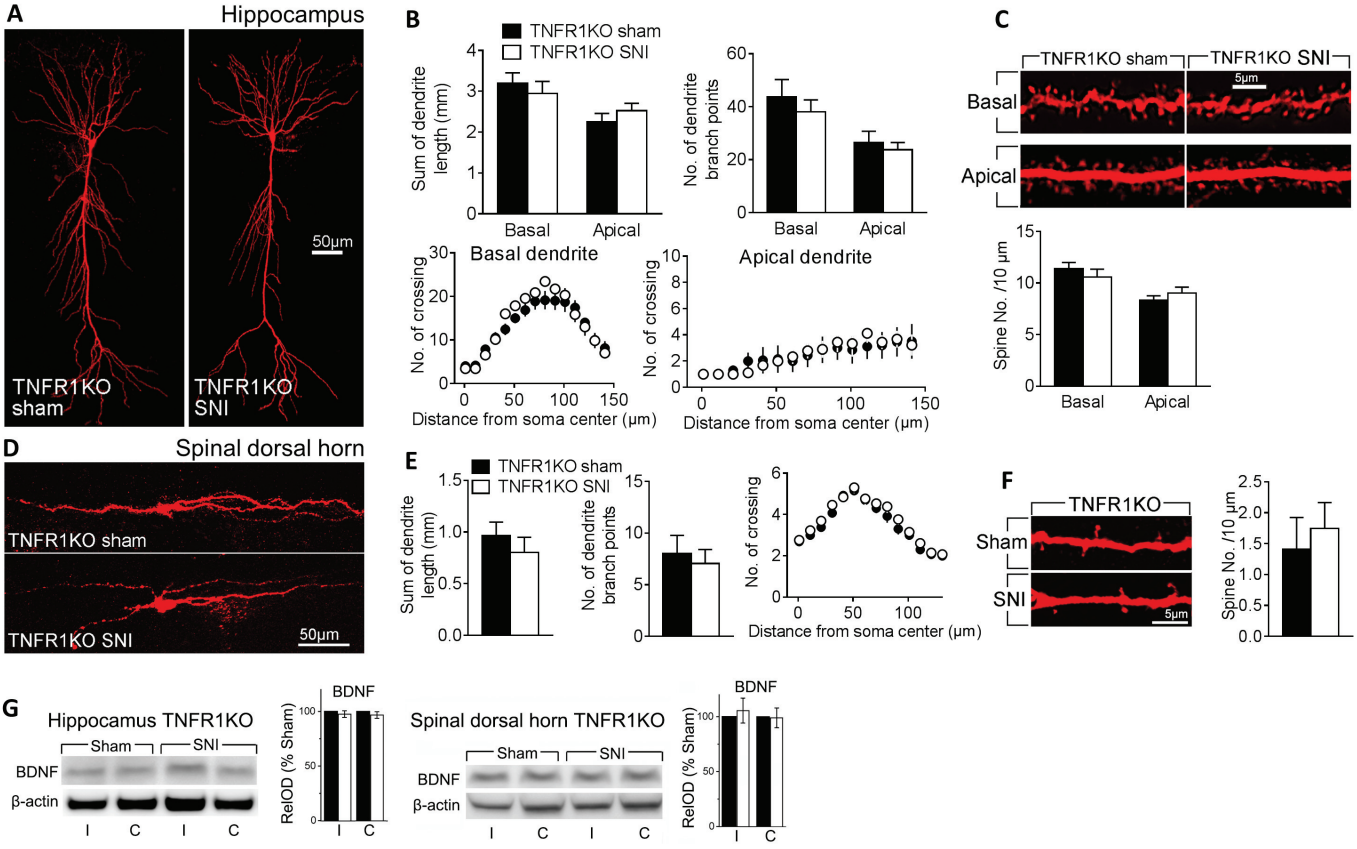

Fig. 4

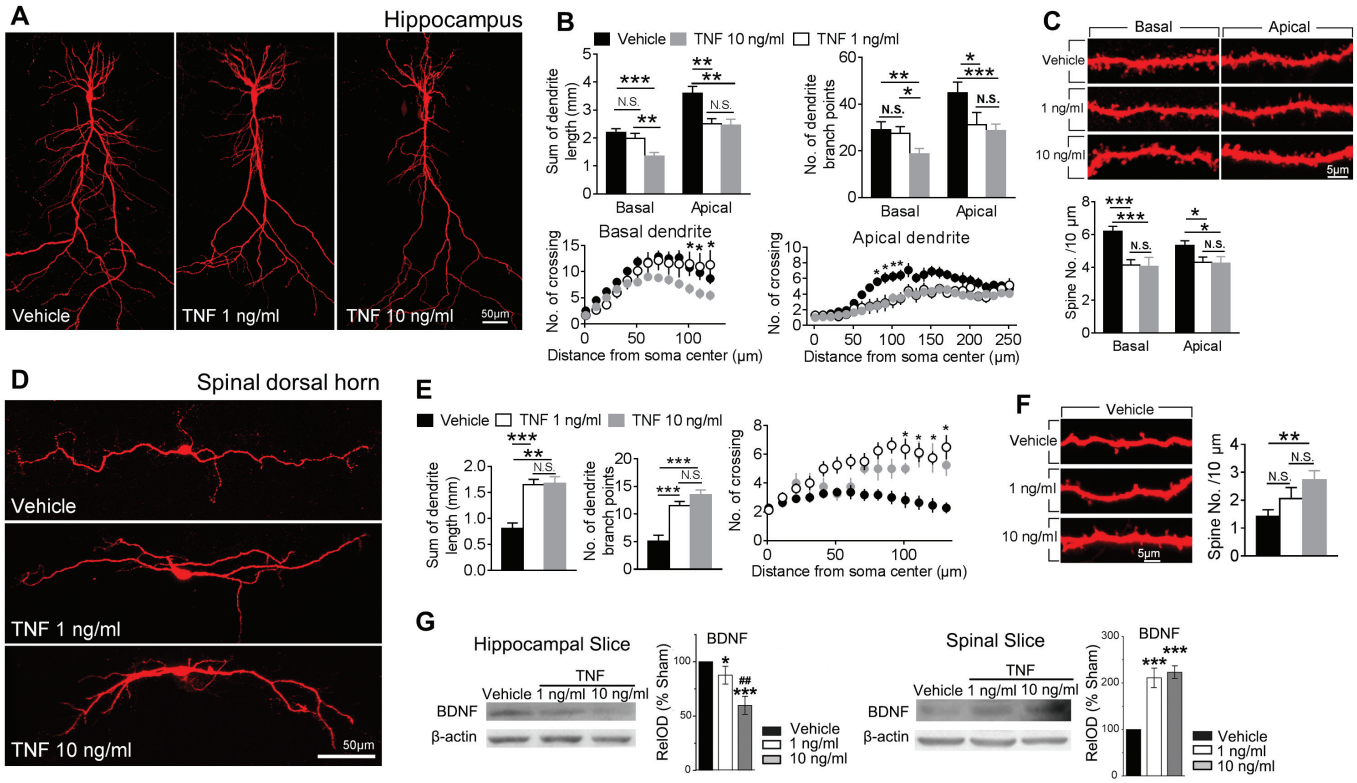

Fig. 5

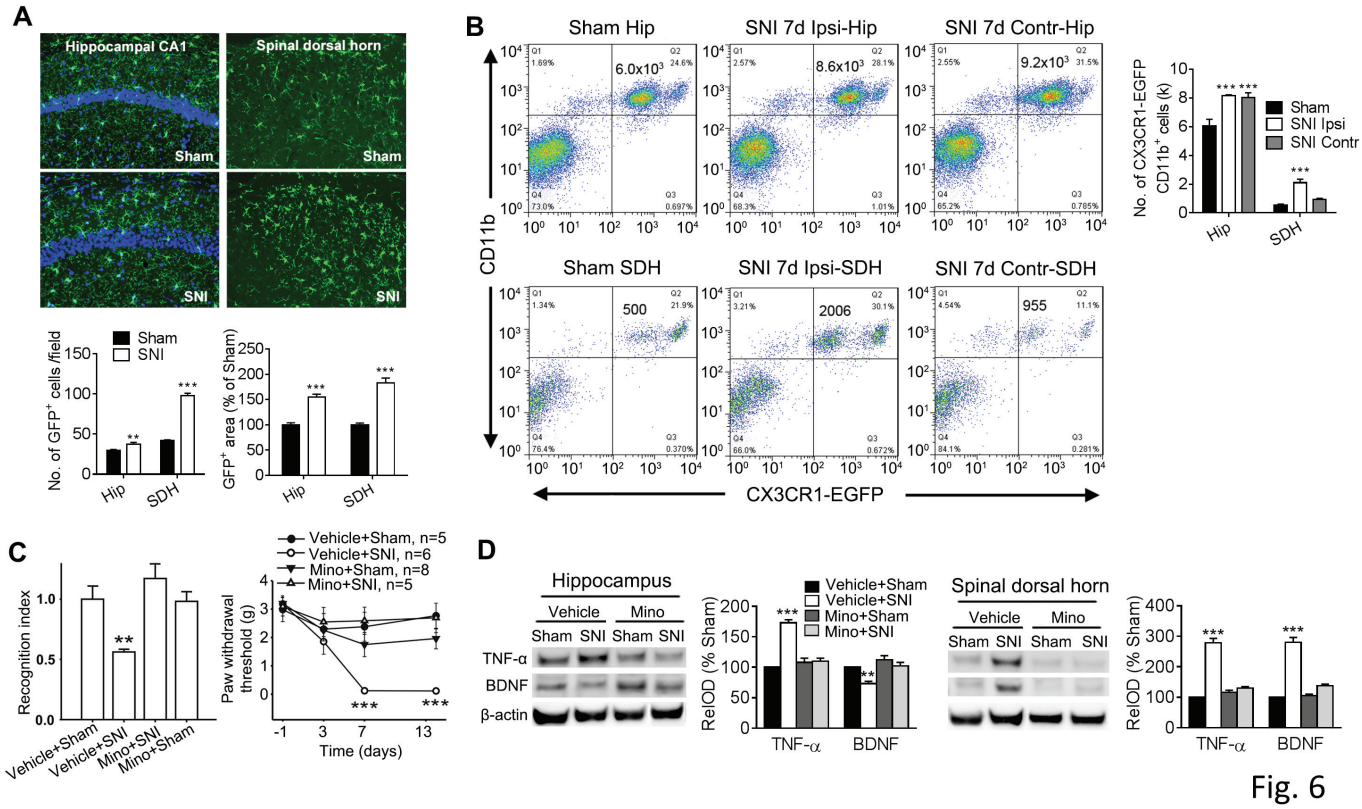

Fig. 6

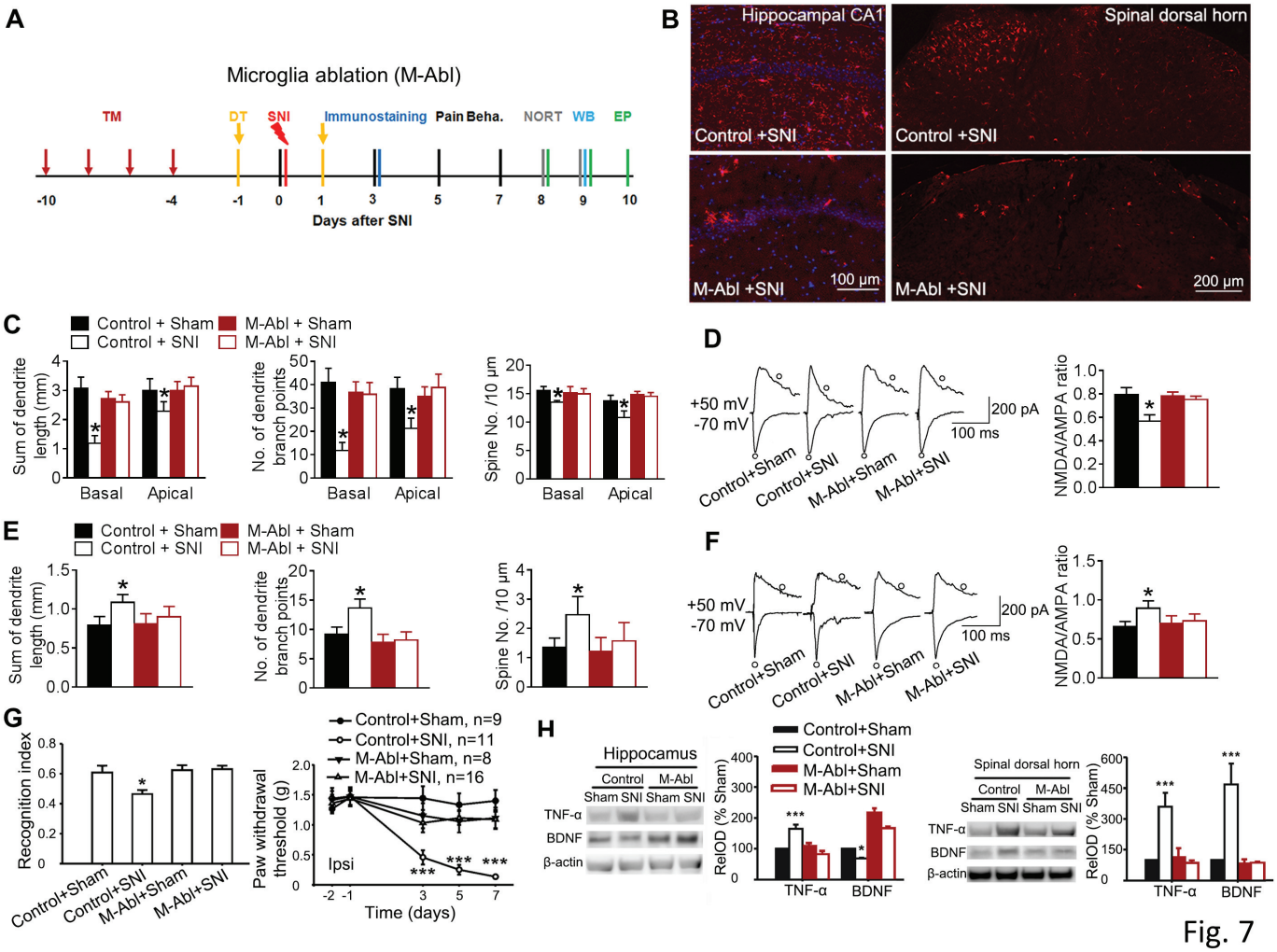

Fig. 7